Electronic Supplementary Material (ESI) for Energy & Environmental Science.

Ionic Thermoelectric Supercapacitor

D. Zhao[a], H. Wang[a], Z. U. Khan[a], J. C. Chen[b], R. Gabrielsson[a], M. P. Jonsson[a], M. Berggren[a] and X. Crispin[a] †

[a.] *Department of Science and Technology,Campus Norrköping, Linköping University,S-60174 Norrköping, Sweden,*

[b.] *Department of Physics, Xiamen University, People's Republic of China*

† *Corresponding author: Xavier.crispin@liu.se*

Supplementary Information includes:

1: Chemical characterization of the PEO-NaOH electrolyte

a) NMR characterization of the PEO-NaOH electrolyte

Proton nuclear magnetic resonance 1H spectra were recorded on Varian (300 MHz) spectrometer. The deuterated solvent was used as internal standard for DMSO-d6 (1H, δ = 2.50) were used as reference. [1] The NMR FID files were analyzed with MestReNova-9.1.0. All PEO samples were analyzed from 15% (w/w) PEO/DMSO-d6.

Table S1 below summarizes the 1H-NMR characterization of the different PEO-Na^+ complexes (entry A-D in Table S1) from the 1H-NMR spectra's (Figure S1). The region between 3.3 ppm and 3.6 ppm are related to hydrogen atoms that are belonging to the (-0-CH_2-CH_2-) polymer chains; while the region at 4.55ppm is identified as hydrogen atom belonging to alcohol end groups for the low molecular weight PEO. The degree of substitution (DS) of the PEO with alcohol end group is about 9%. The significant amount of alcohol groups is a key feature of this liquid polymer. The addition of 3% (w/w) of NaOH (~ 3 mol eq.) to the PEO-400 at rt. (entry B in Table S1) gives a 58% conversion of the alcohol groups -CH_2-OH to alkoxide groups -CH_2-O^-Na^+ through a condensation of water. Heating the same solution to 70 °C for two hours shifts this equilibrium by removal of water to reach a 77% conversion of alcohol protons to sodium ions (entry C in Table S1). Similar results, with metal ions (K^+ and Na^+) transfer ratio (mol%) from solid alkali metal salts of different anions to PEO-400 have been reported by others. [2] To further investigate the role of the anion transfer process on the degree of conversion of protons in PEO-400 to sodium ions, we added NaH (3% w/w, ~ 6 mol eq.) to the PEG-400. The resulting solution showed an almost complete conversion of the protons to sodium ions (entry D in Table S1). The 1H-NMR spectra in figure S1 also show the characteristic peak shifts for the remaining PEO-400 protons, moving from 4.5 ppm in pure PEO-400 to almost 5.5 in PEG/NaH due to PEO-O•••H•••O-PEO interactions, an effect usually seen in DMSO-d6. Although not shown, the 1H-NMR reveals a new contribution at 8.5 ppm upon the addition of NaOH and NaH to PEO, which is attributed to aldehyde groups emerging from the further oxidation of alkoxide groups.

Table. S1 The composition of different PEO-Na^+ complex.

Entry	**Solution composition**	**Peak areas – OH/OCH_2CH_2**	**DS[a]**	**PEG-$[OH]_x$ $[ONa]_y$**
A	Pure PEG	1/22	9.1	100%
B	PEG, NaOH (3% w/w)	1/52	3.8	PEG-$[OH]_{0.42}[ONa]_{0.58}$
C	PEG, NaOH (3% w/w), 70 °C, 2h	1/80	2.5	PEG-$[OH]_{0.23}[ONa]_{0.77}$
D	PEG, NaH (3% w/w)	1/778	0.26	PEG-$[OH]_{0.03}[ONa]_{0.97}$

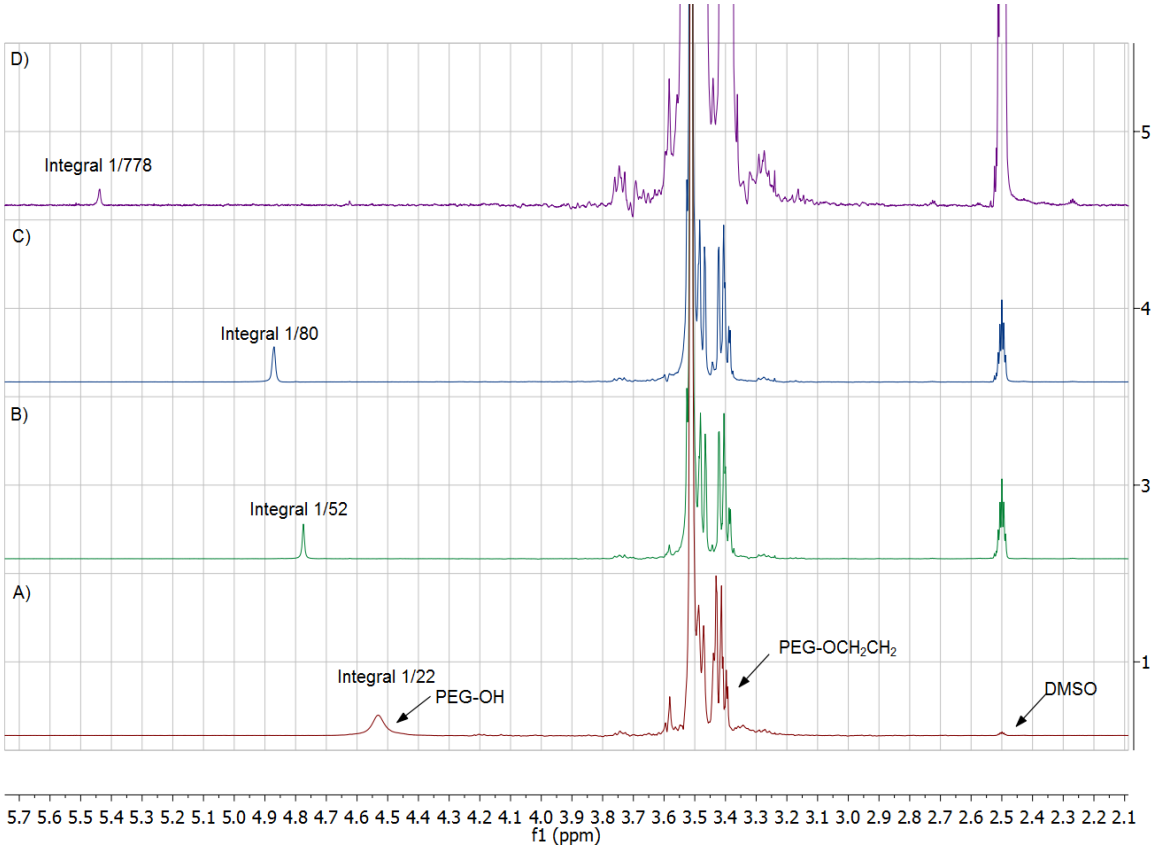

Fig. S1 ^{1}H-NMR spectras of A) Pure PEO, B) PEO-NaOH (3% w/w), PEO-NaOH (3% w/w), 70 °C, 2h, D) PEO-NaH (3% w/w)

b) FTIR characterization of the PEO-NaOH electrolyte

The FTIR (Fourier Transform Infrared Spectroscopy) spectrometer Equinox 55 from Bruker with the ATR (Attenuated Total Reflection) accessory A 225 having diamond crystal was used for studying the absorption of PEO and PEO-NaOH in the range of 400-4000 cm^{-1}. A drop of liquid material was placed on top of the diamond crystal and the measurements were run with 1 cm^{-1} increment for full range (400-4000 cm^{-1}) with 20 scans each time.

The FTIR spectra of pure PEO (Mw=400 g/mol) is compared with that of the PEO-NaOH that is used for the ITESC in the main text (Fig. S2). The PEO sample displays the same features as previously reported in the range 1400-1000 cm^{-1} [3]. As indicated by 1H-NMR; alcohols end moieties are in significant amount and clearly visible by the peak at 3450 cm^{-1} associated to OH stretching (black curve). Possible residual water might also contribute (green curve). Adding the NaOH leads to a decrease of that alcohol $–CH_2$-OH stretching peak around 3400 cm^{-1}, which is associated to the formation of alkoxide $–CH_2$-O^- Na^+: the proton of the alcohol group is removed by adding base. To further verify the result, we substitute NaOH to a stronger base, NaH, which possess higher deprotonating ability. From the result, it is clearly that the peak at 3450 cm^{-1} decrease even more which means most of the proton of the alcohol groups is almost totally removed by the base.

Note also that the presence of a small signal at 1650 cm^{-1} growing upon NaOH and NaH addition is attributed to C=O stretching in an aldehyde. This is supported by the presence of the 1H-NMR contribution at 8 ppm appearing also upon the addition of NaOH and NaH. Alcohol groups in PEO treated in harsh basic environment are known to be transformed from alkoxides to carboxylates (likely through an aldehyde intermediate) [4]. The contribution at 1750 cm^{-1} emerging upon the addition of extra water (green curve) is attributed to the creation of carboxylate groups [4]. In the PEO-NaOH electrolyte used in the ITESC device, the presence of carboxylate is vanishingly small.

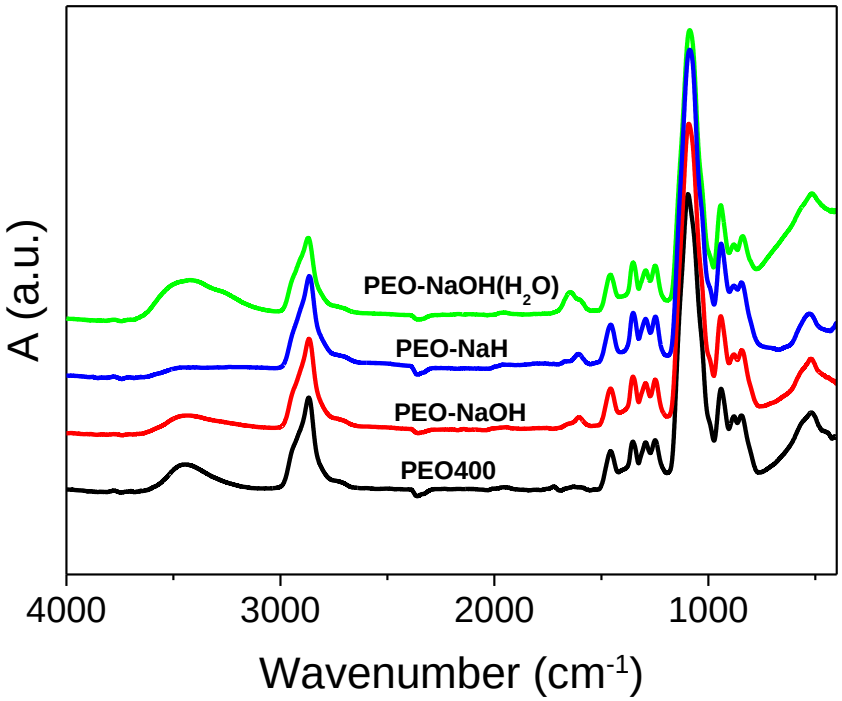

Fig. S2 ATR spectra of PEO (black), PEO-NaOH (70°C, red), PEO-NaH (blue) and PEO-NaOH (green) with a drop of water in the range 400-4000 cm^{-1}.

2: Ionic Conductivity of the PEO-NaOH electrolyte

Dielectric Spectroscopy is a powerful tool for characterizing the electrical and dielectric properties of liquids [5]. Three liquid materials (water, PEO, PEO-NaOH) were characterized inside a standard cell BDS1308 using the Impedance Spectrometer from Novocontrol in the frequency range of 0.1Hz to 10MHz with an input signal of $5mV_{rms}$. The measurements were carried out inside a climate chamber where the temperature was raised from 20 to 80°C with in steps of 10°C.

The Cole-Cole plots of the imaginary (Z´´) and the real part (Z´) of the impedance resemble typical parallel combinations of a resistor and capacitor (Fig. S3). The ionic conductivity was calculated from the first intercept of the high frequency semi-circle, where the response is fully resistive. It can be seen that the semicircle becomes smaller (the intercept is at a lower Z´) as the temperature rises, indicating an increase in the ionic conductivity of the media. For the PEO-NaOH mixture, the bulk conductivity

increases from 7.56E-05 S/cm at 20˚C to 1.96E-03 S/cm at 80˚C and from the Arrhenius plot, the activation energy was calculated to be 476 m eV for the PEO-NaOH mixture.

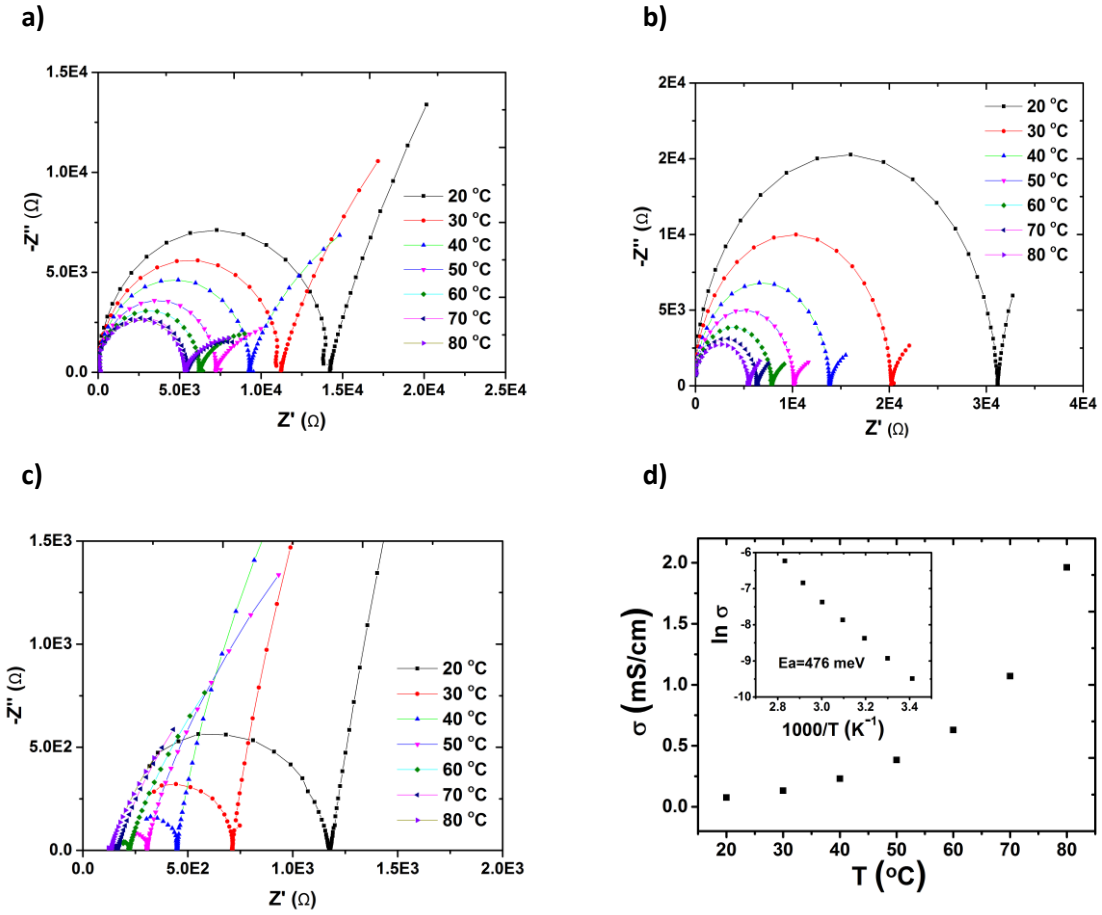

Fig. S3 Cole-Cole plot for **(a)** water (reference), **(b)** PEO and **(c)** PEO-NaOH. **(d)** The ionic conductivity in PEO-NaOH versus temperature (the inset is with other axis scale: log σ vs. 1000/T).

3: Fabrication and calibration of the reference electrodes

The two thermistors of the device consist of gold lines patterned on the substrate (10µm wide, 700mm long), and insulated from the top electrode with a thin (100nm) silicon nitride layer (1000nm). For calibration, the complete device with two thermistors is placed inside a climate chamber, and the two resistors (R_1 and R_2) are measured with four-point probes method using Keithley 2400 at different temperature. Temperature is set at 20, 25, 30, 35, 40˚C, each for 20 min until the resistance keep constant. Fig. S4 shows the slope of the two curves are 88.8 Ω/K and 84.9 Ω/K, which promise an accurate conversion between resistance and temperature. Temperature difference $\Delta T=T_1-T_2$ between the electrodes during Seebeck measurement are subsequently estimated by measuring the resistance of the thermistors.

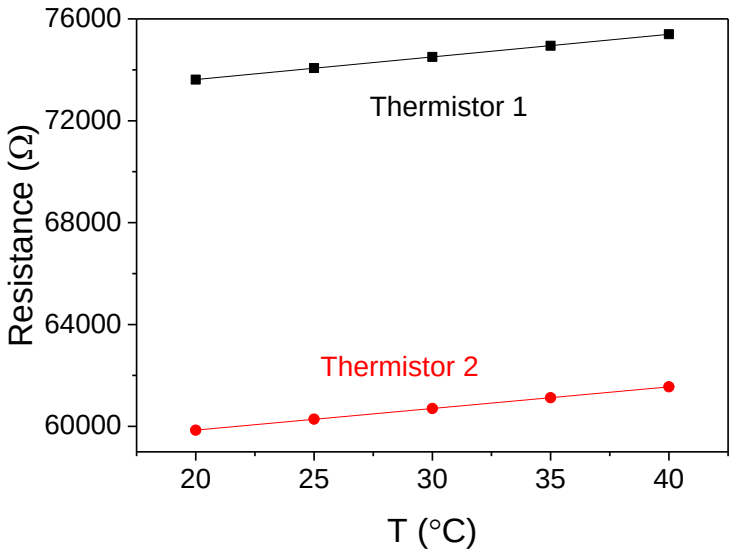

Fig. S4 Calibration curves as the resistance versus temperature for the reference electrodes.

4: Effect of the dielectric constant on the Seebeck coefficient

One question raised in the manuscript was about the effect of the dielectric constant on the heat of transport and Seebeck coefficient of ions. Indeed, the heat of transport of ions is known in aqueous solution [6, 7] but not in PEO. A first indication can be found by using the Born model. In this model, the heat of transport and thus the Seebeck coefficient due to one type of ions is related to both the dielectric constant ε and the variation in dielectric constant as a function of temperature ($d\varepsilon/dT$) is related to the Seebeck co-efficient as:[8]

$$S \propto \frac{d\varepsilon}{\varepsilon^2 dT} \tag{1}$$

Where ε is the complex dielectric constant of the medium and T is the temperature.
From the impedance data presented above (see Fig. S3) and the geometry of the cell, the real ($\acute{\varepsilon}$) and imaginary (ε'') parts of the dielectric constants were calculated using[9]:

$$\varepsilon' = \frac{Z'' L}{2\pi f \varepsilon_0 A Z^2} \tag{2}$$

$$\varepsilon'' = \frac{Z' L}{2\pi f \varepsilon_0 A Z^2} \tag{3}$$

Where L is the length of the cell; A is the area of each electrode; Z', Z'', Z are the real, imaginary and absolute values of the impedances; f is the frequency of the applied voltage; and ε_0 is the permittivity of free space (8.85E-12 F/m).

Fig. S5 displays the real part of the dielectric constant or relative permittivity ($\acute{\varepsilon}$) versus frequency for deionized water (reference) and PEO. The dielectric constant is huge at low frequency due to the formation of electric double layers with the metal electrodes [10]. At high frequency, such phenomenon is absent and the real part of the impedance reaches a constant value from which we

extract the static dielectric constant as *έ* at 1MHz. In order to check our set-up, we first consider DI water as reference. The measured value of the static dielectric constant was 80.6 at 20°C (Fig. S5a) which is very close to the reported value of *έ* (1MHz)=80.1 at the same temperature for pure water [11]. With the same cell, we characterized the PEO liquid (Fig. S5b) and the PEO-NaOH electrolyte (Fig. S5c) and found *έ* (1MHz) =36.1 and 42.5 respectively. We measured the properties at various temperatures and plotted the static dielectric constant versus temperature (Fig. S5d). The slope (*dέ/dT*) for PEO is very small (0.02 K^{-1}) compared to that of water (0.497 K^{-1}). Hence, all in all, one can calculate the product [*dέ/dT*]/(*έ*^{2}) (*Table 2*). According to Born's model, the heat of transport (and Seebeck contribution) by changing from water to PEO should be lower by 5 times. But we measure on the contrary a huge thermovoltage in PEO that cannot obviously be coming from a dielectric effect.

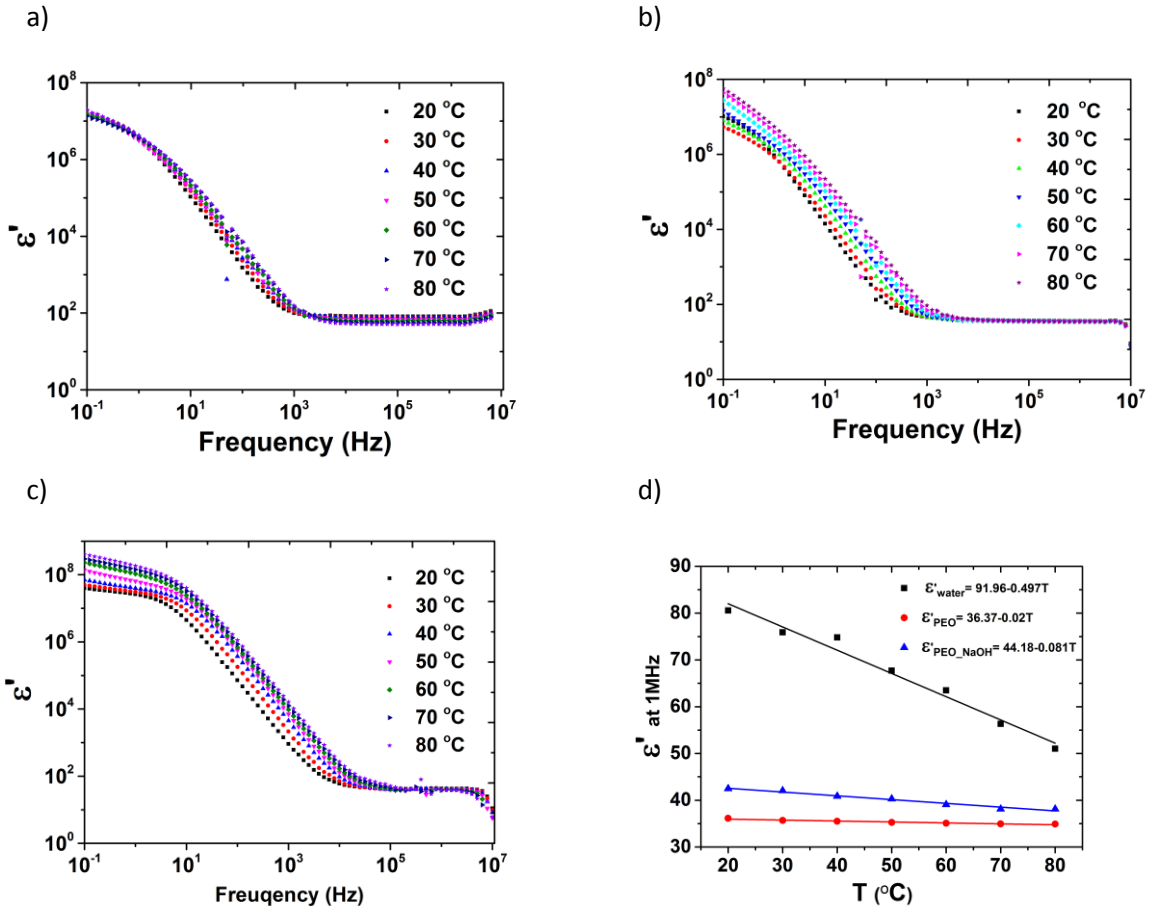

Fig. S5 Real part of the dielectric function as a function of frequency for **(a)** water, **(b)** PEO, **(c)** PEO-NaOH at different temperatures. **(d)** Static dielectric constant *έ* (1MHz) vs. temperature for the three liquids.

Table 2: The static dielectric constant έ of water, PEO, PEO-NaOH and their temperature dependency

Material	*έ at 20°C*	*dέ/dT (K^{-1})*	*[dέ/dT]/(έ^{2}) (K^{-1})*
Water	80.6	-0.497	-7.65E-5
PEO	36.1	-0.02	-1.54E-5
PEO-NaOH	42.5	-0.081	-4.5E-5

5: Thermal conductivity measurement

The thermal conductivity of PEO-NaOH was measured by the three omega (3ω) method. We briefly describe the principle of this electrical method. The 3ω method was initially reported by D.G. Cahill et al. for the thermal conductivity measurement of amorphous materials[12]. A sinusoidal input current at frequency ω causes joule heating in the metal heater, which is in intimate contact with the substrate/material of choice. This causes a fluctuation in the resistance of the metal line at 2ω, which results in a voltage component modulated at 3ω at the terminals of the heater.

The temperature rise (ΔT) at the heater is given by[13]:

$$\Delta T = \frac{P}{\pi l \lambda} \int_0^\infty \frac{Sin^2(kb)}{(kb)^2 (k^2 + q^2)^{1/2}} dk \tag{4}$$

Where *P*, λ are the power input and the thermal conductivity, and *l* and *b* are the length and the half-width of heater, respectively. The thermal penetration depth (1/q) is defined as[12]:

$$\frac{1}{q} = \sqrt{\frac{\lambda}{i2\omega\rho C_p}} = \sqrt{\frac{D}{i2\omega}} \tag{5}$$

Where ρ, C_p and *D* stand for density, specific heat and thermal diffusivity, respectively. As the thermal penetration depth is inversely proportional to the frequency of the input current, it is always necessary to check that the thermal wave remains well within the material at the lowest applied frequency to avoid scattering at the gas-sample boundary.

D.G. Cahill simplified the equation as[9]:

$$\Delta T = \frac{P}{\pi l \lambda} \left[\frac{1}{2} ln \frac{D}{r^2} + ln2 - 0.5772 - \frac{1}{2} ln(2\omega) - \frac{i\pi}{4} \right] \tag{6}$$

Dong-Wook Oh et al.[11] utilized another device architecture designed for the thermal conductivity measurement of liquid samples. We have been inspired by this approach and used it to measure the thermal conductivity of PEO-NaOH solution. The liquid material is filling a plastic cavity designed right above the metal heater deposited on a glass substrate. The temperature oscillation of the heater (ΔT_f) due to the heat transport into liquid material in the cavity can be estimated by subtracting the effect of the substrate as follows[11]:

$$\frac{1}{\Delta T_{s+f}} = \frac{1}{\Delta T_s} + \frac{1}{\Delta T_f} \tag{7}$$

Where ΔT_s is temperature oscillation only with glass and the insulation layer with empty cavity, ΔT_{s+f} is the temperature oscillation of the heater with glass substrate and filled cavity; while ΔT_f is the calculated temperature oscillation due to the heat transported only into the material in the cavity. ΔT_f is used to calculate the thermal conductivity of the PEO-NaOH under study.

We here describe briefly the fabrication and the dimension of the Au heater on the glass substrate. The glass substrate was coated with 15 nm chrome (Cr) and 140 nm gold (Au) and patterned by photolithography to get a 3 mm long and 20 µm wide Au line (the heater-thermometer). This metal line was then insulated with a 2 µm thick UV cured SU8 layer. The metal heater-thermometer was first calibrated inside a climate chamber by varying the temperature from 20°C to 50°C. Then in order to measureΔT_s, the glass sample with insulation and empty cavity was placed inside a vacuum cryogenic probe station (Janis Research) to avoid gas convection effect. An input AC current was applied from a waveform generator (3022C Tektronix) and the 3ω voltage was measured by a Lock-in Amplifier (SR850 Stanford Research) with a precision difference amplifier AD8279 for signal conditioning. The measured 3ω voltage was translated to ΔT_s by[14]:

$$\Delta T_s = 2\frac{V_{3\omega}}{I}\frac{\partial T}{\partial R} \tag{8}$$

The results of ΔT vs. *ln2ω* are plotted in Fig. S6 for empty and the cavity filled with different materials. All the 3ω measurements were carried out with the same input current for the same frequency range. The cavity was 1 cm tall and it was filled with 2 mL of liquid in each case. It can be seen in all measurements that the total temperature oscillation ΔT_{s+f} is smaller than ΔT_s since part of the heat generated by the heater penetrates into the solution. The temperature oscillation ΔT_f due to the heat propagated into solution only was calculated using equation (8) and the thermal conductivity was calculated from a linear fit of ΔT_f vs. *ln2ω*. The validity and accuracy of our experimental setup was first tested with known materials (DI water and ethylene glycol (EG)). Two measurements were carried out by filling the cavity with water and then with ethylene glycol (EG). The measured values of the thermal conductivities of 0.632 $Wm^{-1}K^{-1}$ (water) and 0.272 $Wm^{-1}K^{-1}$ (EG) are in agreement with the reported values of 0.6 $Wm^{-1}K^{-1}$ and 0.27 $Wm^{-1}K^{-1}$ [11]. Hence, the measurement setup was trustable with an uncertainty of ±5%. Finally, the cavity was filled with PEO and then with PEO-NaOH and the calculated thermal conductivities were 0.191 $Wm^{-1}K^{-1}$ and 0.216 $Wm^{-1}K^{-1}$, respectively.

a)

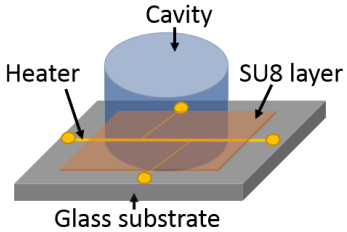

b)

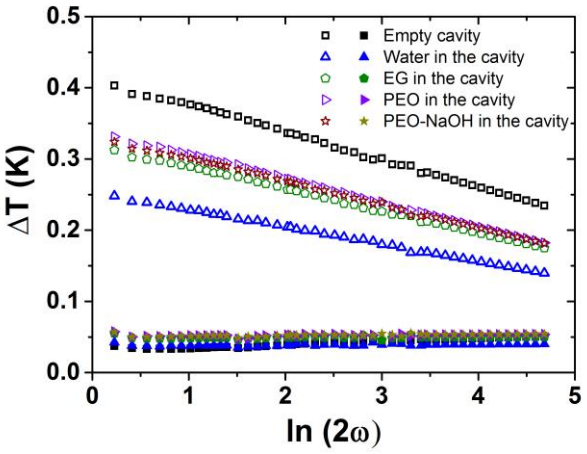

Fig. S6 **(a)** Sample structure, **(b)** Temperature oscillation on the gold (Au) heater. Empty symbols are for the in phase and filled symbols are for the out of phase components of ΔT.

6: Preparation of self-assembled CNT electrode on Au

CNT was dispersed in water to form a 0.1 % concentration solution, and exposed to ultrasonic treating for 30 min. The Au electrodes were pretreated by UV plasma for 3 min, and placed on a hot plate set at 105°C. Next, a certain amount of CNT solution is dipped on Au electrode during heating (30 µL for thin CNT electrodes, and 60 µL for thick CNT electrodes). After water evaporation, the CNT attached to the surface of Au due to hydrophobic forces between the two. The prepared electrodes were rinsed by acetone and water before use.

7: Self-discharge of devices using both thick and thin CNT electrodes

The self-discharge is investigated in detail by monitoring the open voltage (V_{open}) of the capacitors after electrical charging. As shown in fig S7, devices with thin and thick CNT electrodes are charged electrically at three different potentials (50 mV, 100 mV and 150 mV). Next, the circuit is cut and V_{open} is recorded versus time. Initially, V_{open} decreases rapidly, especially for the devices with thin CNT eletrodes. And the inset figure shows that for the same electrodes, the decay rate of different charging potential are similar.

The electrically charged SCs, which could be discharged directly (time=1 s) after charging, provide $Q_{discharge}/Q_{charge}$ of 94% and 83% for the thick and thin CNT electrode devices, respectively (see table 1). However, if discharging is triggered after a time equal to the equilibration time t_{eq}, i.e. accounting for the self-discharge, this gives $Q_{discharge}/Q_{charge}$ of 28% (thick CNT electrodes), which is very close to the measured 27% in the ITEC. Since the thick CNT electrode possess more compensate charge during charging, it needs longer time for self-discharge. This explains why the delay curve is sharper for the thin electrode than the thick CNT electrode.

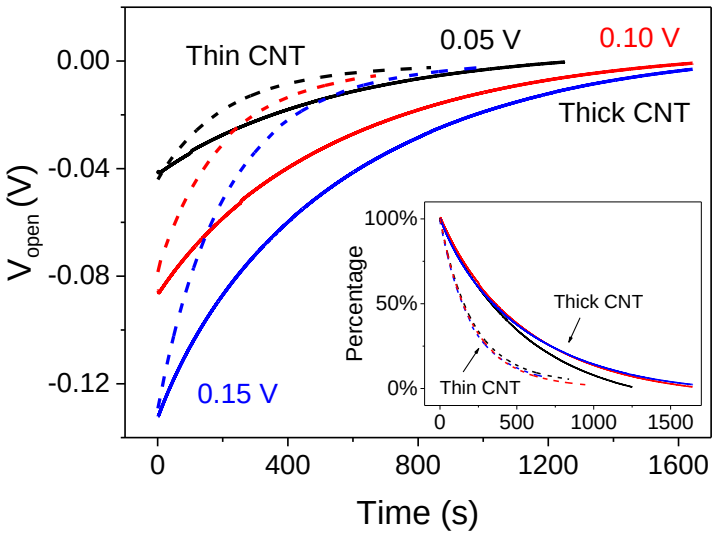

Fig. S7 Decay of V_{open} after electrical charging at 0.15 V (blue), 0.10 V (red) and 0.05 V (black), for supercapacitors based on thin (dashed lines) and thick (solid lines) CNT electrodes.

8: Charging current comparison and control measurement using Au electrodes.

The charging current is measured for both electric and thermoelectric charging. For thermoelectric charging, ΔT=4.5 K gives a V_{thermo} of 0.05 V. After V_{thermo} has stabilized, the load resistance is connected. For electric charging, the charging potential is set the same as V_{thermo} for thermoelectric charging (0.05 V). The device is placed in a climate chamber to keep the same temperature as $T_{average} = \frac{T_{hot}+T_{cold}}{2}$. From the results shown in fig. S8 a, the charging behavior and leakage current of the two methods are almost the same.

Fig. S8 b shows the charging and discharging performance of a device with Au electrodes (no CNTs). After connecting R_{load}, V_{thermo} drops immediately because of the small capacitance. Because there are no compensate charges on the electrodes, V_{thermo} tends to first approach its original value and then decrease to zero when R_{load} is disconnected and the heat is turned off.

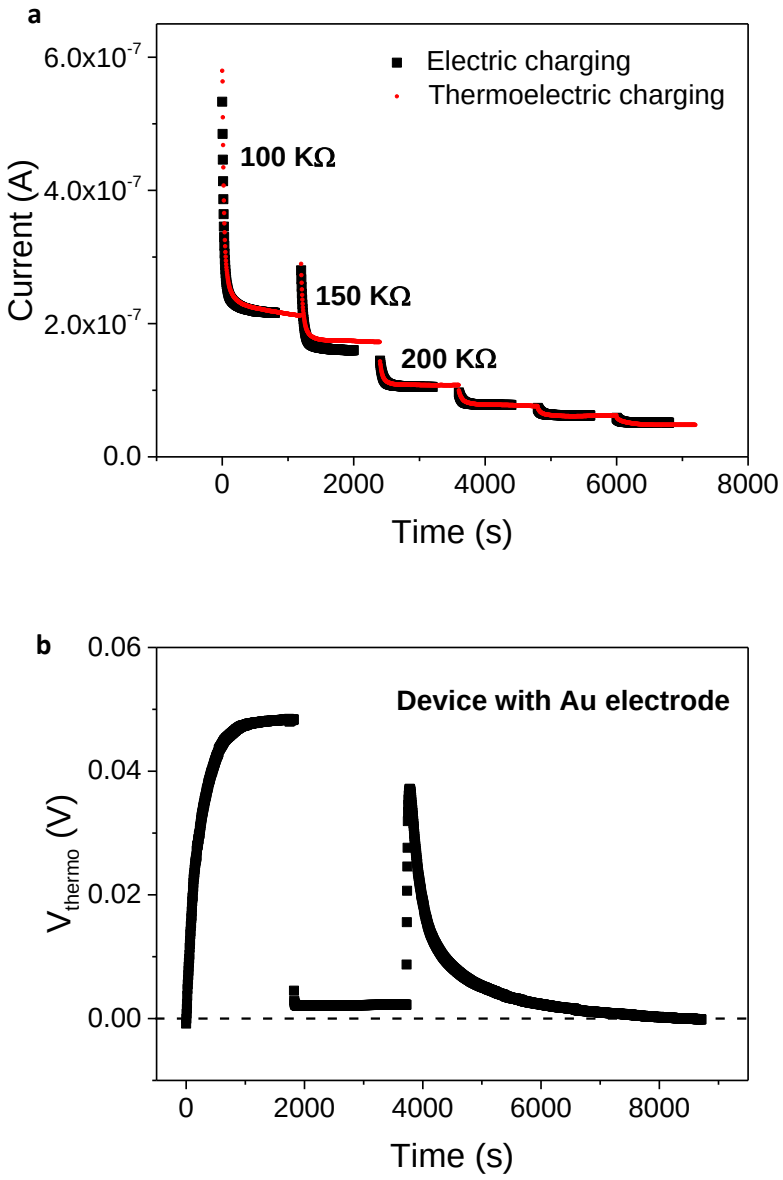

Fig. S8 **(a)** Comparison between electric and thermoelectric charging current for different R_{load}. **(b)** Charging and discharging measurement using Au electrodes.

9: Full mathematical framework to describe the equivalent circuit

According to the equivalent circuit, the charging electric current $I(q_{ch} = \frac{dq_{ch}(t)}{dt})$ and the discharging electric current $I(q_{dis}) = -\frac{dq_{dis}(t)}{dt} = -C\frac{dV_{dis}(t)}{dt}$ can be calculated from the following equations:

$$(R_s + R_{load})\frac{dq_{ch}(t)}{dt} + [1 + \frac{(R_s + R_{load})}{R_p}]\frac{q_{ch}(t)}{C} = \alpha_i \Delta T \qquad (1)$$

From Eq. (1), we can obtain

$$q_{ch}(t) = q_{ch}(0)\exp\{-[\frac{1}{C(R_s + R_{load})} + \frac{1}{CR_P}]\}t$$
$$+\frac{\alpha_i \Delta T / (R_s + R_{load})}{\frac{1}{C(R_s + R_{load})} + \frac{1}{CR_P}}\left(1 - \exp\{-[\frac{1}{C(R_s + R_{load})} + \frac{1}{CR_P}]\}t\right) \quad \text{Eq. 2a}$$

$$\tau = \frac{C(R_S + R_{load})R_p}{R_S + R_{load} + R_p}, \text{ when } R_P >> (R_s + R_{load}), \tau = C(R_s + R_{load}). \quad \text{Eq. 2b}$$

$$q_{ch}(t) \approx q_{ch}(0)\exp(-t/\tau) + C\alpha_i \Delta T[1 - \exp(-t/\tau)] \quad \text{Eq. 2c}$$

In the experimental charging and discharging processes, t is finite. $q_{ch}(0) > 0$ except for the first charging process. $q_{ch}(0)$ is dependent on the time of the charging and discharging processes. We take 5 times of τ as the charging and discharging time, for during this period, 99% of the charge has been transferred.

10: Charging current

The voltage across R_{load} is measured for different R_{load}, and the charging current is obtained by $I = \frac{V}{R_{load}}$. To calculate the amount of charge and energy stored in the device, the curve of the current is integrated for the charging period. For each R_{load}, the complete charging time is considered as 5 times of the time constant (τ).

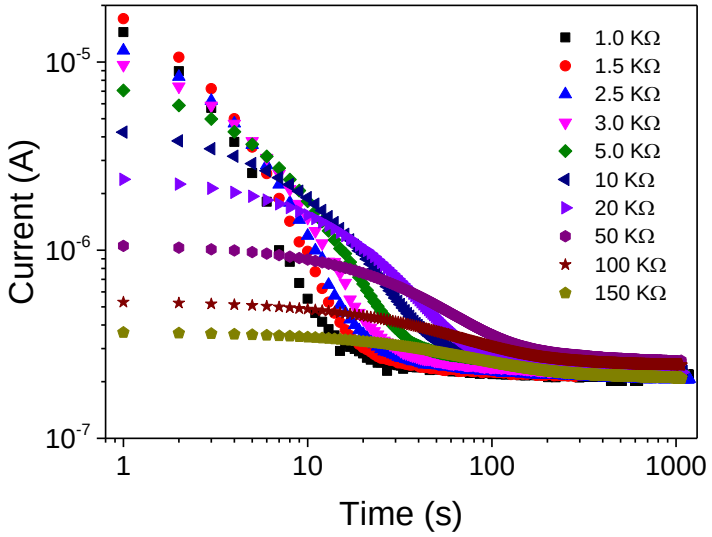

Fig. S9 Current generated during charging for serious R_{load}, plotted with time.

11: Efficiency

Heat-to-electricity charging conversion efficiency

We evaluate the efficiency of the ITESC in converting heat to electricity through the charging efficiency. The charging efficiency is defined as the ratio between the electrical energy that is generated and stored in the ITESC from the charging (E_{out}, term A below) and the total heat that is required to achieve that storage and hence, the total heat absorbed over one full ITESC cycle (Q_{in}). Experimentally, A is measured as the integrated current through R_{load} minus the leakage current during charging (step ii in Fig 3a), $\frac{1}{2C}\left(\int_0^{t_{ch}} I_{ch}dt\right)^2$. Term A can also be calculated from the measured device capacitance and the effective charging voltage as $\frac{1}{2}C[\Delta T\alpha_i - V_{load} - V_s]^2$.

$$\eta = \frac{E_{out}}{Q_{in}} = \frac{\frac{1}{2}C[\Delta T\alpha_i - V_{load} - V_s]^2}{\frac{1}{2}mC_h\Delta T + \kappa\frac{A}{L}\int_0^{t_{st}}\Delta T dt + \kappa\frac{A}{L}\int_{t_{st}}^{t_{ch}}\Delta T dt - \frac{1}{4}\frac{R_s C(\Delta T\alpha_i - V_{load} - V_s)^2}{R_{load}} + CT_h\alpha_i^2\Delta T}$$

$$= \frac{A}{B+C1+C2+D+E} \qquad (3)$$

Q_{in} has several types of contribution. First, $\frac{1}{2}mC_h\Delta T$ (term B) is the heat absorbed by the PEO-NaOH electrolyte (mass m=9.4×10^{-2}gr, specific heat C_h= 2.13 Jg^{-1}K^{-1} (from the datasheet of DOW chemical company) upon increasing the average temperature of the electrolyte (note that the mass of the electrodes is negligible ~10^{-6}gr compared to the mass of PEO-NaOH). Second, the Fourier contribution $\kappa\frac{A}{L}\int_0^{t_{st}}\Delta T dt$ (term C1) corresponds to the heat flow during the time to establish the steady-state thermovoltage (step i in Fig. 3a) and the term C2 is the heat flow during charging. The thermal conductivity κ of PEO-NaOH is 0.21Wm^{-1}K^{-1}. Third, the Joule effect (term D), equal to $\frac{1}{4}\frac{R_s R_p C(\Delta T\alpha_i - V_{load} - V_s)^2}{(R_{load}+R_s)(R_{load}+R_s+R_p)}$, will bring back part of the energy and lower the absorbed heat. Experimentally, we measure term E as $\frac{1}{2}R_s\int_0^{t_{ch}} I_{ch}^2 dt$, where R_s is the internal resistance of the ITESC and I_{ch} is the charging current equals to I_{load}-$I_{leakage}$. Finally, the ionic current also lead to a small Peltier heat contribution $CT_h\alpha_i^2\Delta T$ measured as $\alpha_i T_h\int_0^{t_{ch}} I_{ch}dt$ (term E). The charging efficiency for different R_{load} is shown in Fig. S11 a (symbols are from the current measurement and lines are from calculation) for ΔT=4.5 K and reaches 6× 10^{-6} % at low R_{load}.

We compare the efficiency of the ITESC with that of a circuit composed of a SC connected in series with a conventional TEG. In that case, we take a TEG of the same area and volume as the ITESC but made of Bi_2Te_3 and submitted to ΔT=4.5K. Using the same heat power for ITESC, we have measured the time needed to establish a constant open circuit potential (t_{st}) for the Bi_2Te_3 leg to be 10 times lower than for the ITESC of the same dimension. This time t_{st} for Bi_2Te_3 is limited by the heat diffusion; while for the ITESC t_{st} is limited by the ionic thermodiffusion (slower than the heat diffusion). Using the material properties of Bi_2Te_3 (C_h= 0.153Jg^{-1}K^{-1}, m=0.60g, κ=1.2Wm^{-1}K^{-1}), we calculate the new terms B, C1 and C2. As far as the terms A, D and E are concerned, we assume this is from SC based on CNT and PEO-NaOH (see main text section 2) but charged with the thermovoltage of the TEG. As shown in Figure S10 a, the efficiency of the TEG-SC (curve iii) is more than 2500 times lower than the efficiency of the ITESC (curve i).

Since this is the first ITESC and that we don't have optimized its architecture, the efficiency is far from what may be provided by future devices. In order to investigate the potential for

improvement, we plot the various energetic contributions corresponding to the terms in equation 3 (Fig. S10 b). The dominating contribution is from the heating energy (term C), because the time needed for the electrolyte to reach a stable V_{open} (t_{st}) is relatively long. In turn, t_{st} can likely be decreased by a factor of 10000 by reducing the length of the electrolyte leg from 1 mm to 10µm. Because the time needed to reach steady thermovoltage (t_{st}, region i in Fig 3a) depends quadratically on the length of the leg since this is a diffusion limited phenomenon [15]. Note that with an active external cooling power of 8W, a temperature gradient ΔT=4.5K is obtained over a 10 µm long PEO-NaOH leg. Simultaneously, the heat flux will increase by a factor of 100 due to Fourier equation: $Q = \kappa A \frac{\Delta T}{L}$. Hence, decreasing the length by two orders of magnitude leads to two orders of magnitude reduction of C1. Replacing the 1 mm long leg with a 10 µm long leg leads to a reduction in term B; which results in an enhancement of efficiency from 6×10^{-6}% to 3×10^{-4}% (curve ii). We now turn to the efficiency of the TEG-SC circuit, using the material parameters for Bi_2Te_3 for a 10µm long leg of the same volume as PEO-NaOH in ITESC. Note that because of the higher thermal conductivity, a cooling power of 48W is now required to get a temperature gradient of 4.5K. The efficiency of the TEG-SC (curve iv) reaches 2×10^{-8} % and is around 11000 times lower than the ITESC (curve ii).

Fig. S10 c reports the predicted evolution of the efficiency (with a 10 µm long leg) over the wide range of temperature gradient (0-100°C). Because the numerator in Equation 4 scales as ΔT^2 and the denominator is dominated by the terms B+C1+C2, which are proportional to ΔT, the resulting efficiency is linearly increasing with ΔT. It is important to keep in mind that the required external cooling-heating power increases proportionally with ΔT, so ΔT=100°C would require 177W. We observe that the efficiency increases with ΔT to around 0.01% at ΔT=100°C. The efficiency for TEG-SC also increases with ΔT, however, remains more than three orders of magnitude lower than the efficiency of the ITESC for all investigated ΔT. Moreover, for electrolyte possesses higher conductivity, which means a lower Rs, the time needed for fully charging will be shortened. And this will result an enhancement of efficiency to 0.08%.

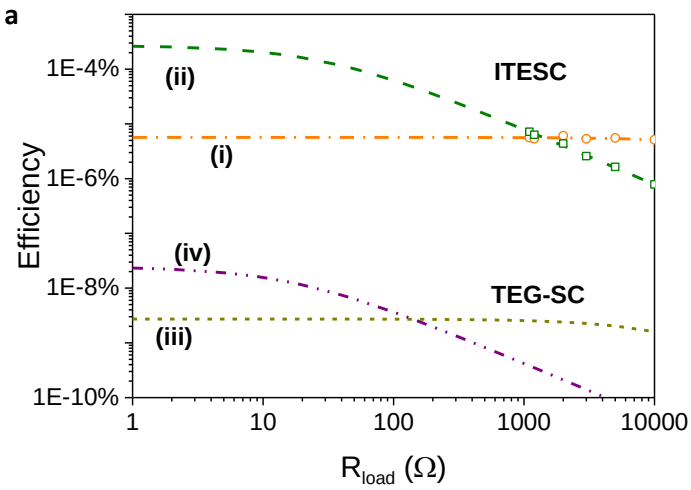

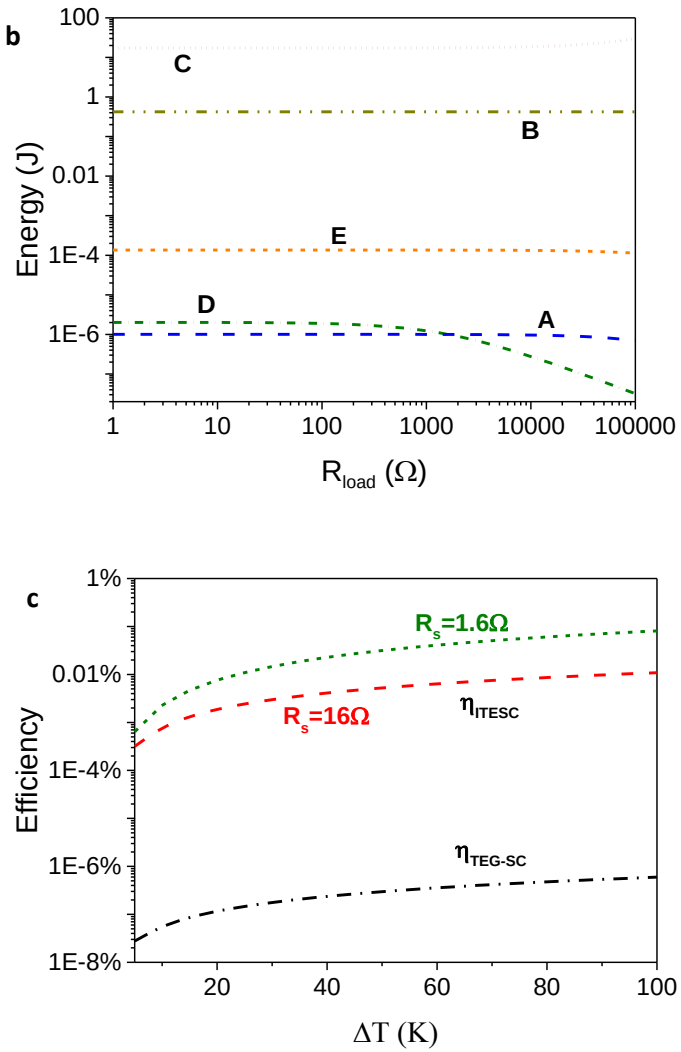

Fig. S10 (a) The efficiency of ITESC and TEG-SC for different R_{load} with consideration of: the length of leg we are using (i: ITESC, iii: TEG-SC); the length of leg is reduced from 1 mm to 10 μm (ii: ITESC, iv: TEG-SC). **b**, The contribution of the four different parts of the input energy, and the output energy. **c,** Predicted efficiency of ITESC (red dashed line) and TEG-SC (black dashed-dotted line) versus Δ*T*, and electrolyte of 10 times higher conductivity (green short dashed line), with leg length of 10 μm.

References:

1. Gottlieb, H.E., Kotlyar, V. & Nudelman, A. NMR chemical shifts of common laboratory solvents as trace impurities. *J Org Chem*. **62.** 7512-7515 (1997)
2. Chen, J., Spear, S. K., Huddleston, J. G. & Rogers, R. D. Polyethylene glycol and solutions of polyethylene glycol as green reaction media. *Green. Chem*., **7**, 64-82 (2005)
3. Su, Y.l., Wang, J. & Liu,H.Z. FTIR spectroscopic investigation of effects of temperature and concentration on PEO−PPO−PEO block copolymer properties in aqueous solutions. *Macromolecules*, **35**, 6426-6431 (2002)
4. Xiao, Y., Jiang, J. & Huang, H. *C*hemical dechlorination of hexachlorobenzene with polyethylene glycol and hydroxide: Dominant effect of temperature and ionic potential. *Scientific reports*, **4**. DOI:10.1038/srep06305 (2014)
5. Blythe, A.R. & Bloor, D. Electrical properties of polymers2005: Cambridge University Press.
6. Agar, J., Mou, C. & Lin, J.L. Single-ion heat of transport in electrolyte solutions: a hydrodynamic theory. *The Journal of Physical Chemistry*. **93**(5) 2079-2082 (1989)
7. Sokolov, V., Kobenin,V. & Usatchova, I. The standard entropy of transport of potassium chloride in the water–methanol system at 298 K*. Physical Chemistry Chemical Physics* **1**(12) 2985-2987 (1999)
8. Bonetti, M., Nakamae, S., Roger, M. & Guenoun, P. Huge Seebeck coefficients in nonaqueous electrolytes*. The Journal of chemical physics*, **134**(11) 114513 (2011)
9. Lanfredi, S. & Rodrigues, A. Impedance spectroscopy study of the electrical conductivity and dielectric constant of polycrystalline $LiNbO_3$. *Journal of applied physics,* **86**(4) 2215-2219 (1999)
10. Bordi, F., Cametti, C. & Colby, R. Dielectric spectroscopy and conductivity of polyelectrolyte solutions*. Journal of Physics: Condensed Matter*, **16**(49) R1423 (2004)
11. Malmberg, C. & Maryott, A. Dielectric Constant of Water from 00 to 1000 C*. Journal of research of the National Bureau of Standards*, **56** 1-8 (1956)
12. Cahill, D.G. & Pohl, R.O. Thermal conductivity of amorphous solids above the plateau*. Physical Review B*, **35**(8) 4067-4073 (1987)
13. Cahill, D.G., Thermal conductivity measurement from 30 to 750 K: the 3ω method*. Review of Scientific Instruments*, **61**(2) 802-808 (1990)
14. Oh, D.W., Jain, A., Eaton, J. K., Goodson, K. E., & Lee J. S. Thermal conductivity measurement and sedimentation detection of aluminum oxide nanofluids by using the 3ω method. *International Journal of Heat and Fluid Flow*, **29**(5) 1456-1461 (2008)
15. Atkins, P. and J. de Paula, *Atkins' Physical Chemistry*. 2010: OUP Oxford.